Formation of surface structures during heteroepitaxial thin film growth on prepatterned substrates

P. Liu and C. Lu
Institute of High Performance Computing, Singapore 117528, Singapore

Y. W. Zhang*
Department of Materials Science and Engineering, National University of Singapore, Singapore 119260, Singapore

(Received 2 March 2007; revised manuscript received 1 June 2007; published 22 August 2007)

Guided quantum dot self-assembly grown heteroepitaxially on a substrate surface prepatterned with cosine-like humps is studied by computer simulation. The SiGe/Si material system is used as a model system, in which the strain energy, surface energy, wetting effect, surface anisotropy, and elastic anisotropy are taken into account. The simulation results reveal the formation of surface structures which may potentially be of practical applications.

DOI: 10.1103/PhysRevB.76.085336 PACS number(s): 81.15.Aa, 68.55.Ac, 68.65.Hb

INTRODUCTION

Much experimental,[1–8] modeling, and simulation[9–20] effort has been made to achieve ordered quantum dot arrays through self-assembly; however, there are still many unresolved issues regarding the kinetics and thermodynamics underlying the quantum dot formation and self-assembly. Ge and SiGe on Si(001) or InGaAs on GaNi(001) systems have been commonly used as a model system for understanding these issues. However, even in these seemingly simple systems, the epitaxial processes are proved to be extremely complex.[11]

Quantum dot arrays with precisely controlled positions and sizes are desirable for making the template for micro- and nanoelectronic devices.[21,22] Numerous experimental works have shown that unguided self-assembled growth of quantum dots usually fails to realize perfectly ordered dot arrays.[2–7] Recently much effort has been shifted to use guided self-assembly through prepatterning, and several prepatterning methods have been reported, including selective epitaxial growth in oxidized windows,[23–28] buried stress fields due to ion implantation,[29,30] surface roughening through cooperative island formation,[29,31] and electron beam lithography with subsequent reactive ion etching.[32–34] These prepatterned substrate surfaces are usually manifested with either ordered concave pits, or ordered convex humps, or regular strain energy profiles. It is expected that at each pit or hump, a single quantum dot can form after the subsequent growth, resulting in a one pit (hump)-one dot relation. In reality, quantum dots have been found to nucleate at different positions even if an ordered prepatterned substrate is used, often failing to produce the one-to-one relation.[35] Hence the method to reliably and reproducibly achieve ordered quantum dot arrays through surface prepatterning is still not known. The surface roughening process and its subsequent island formation may be qualitatively understood by a simplified energetic argument[36–38]; however, it is found that other factors, such as the surface energy anisotropy, elastic anisotropy, wetting effect, and surface prepatterning, are also influential.[1–6,39–42]

A continuum framework is employed here to demonstrate the formation of distinctive surface patterns obtained by prepatterning a substrate surface into a regular hump array. It is shown that the combined effect of the substrate surface prepatterning, surface energy anisotropy, and elastic anisotropy is essential in forming surface patterns, elucidating interesting kinetic pathways for guided self-assembly of quantum surface structures.

MODEL FORMULATION

The mismatch strain ε_0 for an elastically anisotropic thin film with lattice spacing a_f heteroepitaxially grown on an elastically anisotropic substrate with lattice spacing a_s is defined as $\varepsilon_0=(a_f-a_s)/a_s$. For simplicity, one may neglect the mismatch of elastic properties between the substrate and the film, and assume that the film and substrate have the same elastic properties. Surface mass diffusion and condensation are related to the magnitude of the surface chemical potential. The surface chemical potential for a strained film surface can be written as

$$\chi = \chi_0 + \Omega\left(\omega - \kappa\gamma + \nabla_s \cdot \frac{\partial \gamma}{\partial \mathbf{n}}\right), \tag{1}$$

where χ_0 is the reference chemical potential, Ω is the atomic volume of the diffusive atom, $\omega=\sigma_{ij}\varepsilon_{ij}/2$ is the strain energy density, κ is the mean curvature, γ is the film surface energy, $\mathbf{n}$ is the surface unit normal vector, and ∇_s is the surface gradient operator. It is seen that surface energy anisotropy is included in the chemical potential. A linear elastic relation between the stress and strain is assumed in the present treatment, i.e., $\sigma_{ij}=C_{ijkl}\varepsilon_{kl}$, where C_{ijkl} is the component of the elastic modulus tensor, σ_{ij} is the component of the stress tensor, and ε_{kl} is the component of the strain tensor. For cubic crystalline materials, there are three independent elastic constants: C_{11}, C_{12}, and C_{44}, which are related to Young's modulus E, Poisson's ratio ν, and the elastic anisotropy strength A by $E=(C_{11}^2+C_{11}C_{12}-2C_{12}^2)/(C_{11}+C_{12})$, $\nu=C_{12}/(C_{11}+C_{12})$, and $A=2C_{44}/(C_{11}-C_{12})$.

It is known that the deposition flux is dependent on the difference between the chemical potential of the vapor phase and that of the film surface. The growth rate of the thin film

 ©2007 The American Physical Society

surface, v_g to the first-order approximation, is assumed to be proportional to the difference between the chemical potential of the vapor phase, $\chi_0+\chi_v$, and the surface chemical potential, χ, i.e.,

$$v_g = g(\chi_0 + \chi_v - \chi), \tag{2}$$

where g is a growth parameter, which depends on the sticking coefficient, temperature, and the mass of the vapor particle. It is noted that χ_v is the chemical potential of the vapor phase relative to χ_0, the reference chemical potential.

Both surface diffusion and condensation contribute to the evolution of the film surface. The surface evolution rate based on the conservation of mass can be written as

$$v_n = D\nabla_s^2\chi + g(\chi_0 + \chi_v - \chi), \tag{3}$$

where v_n is the normal velocity, $D=D_s\delta_s/k_BT_s$, D_s is the surface diffusion coefficient, δ_s is the diffusive layer thickness, k_B is the Boltzmann constant, T_s is the absolute temperature, and $\nabla_s^2=\nabla_s\cdot\nabla_s$ is the surface Laplacian. Equation (3) may be solved for v_n using the finite element method.[42]

The surface energy is assumed to be of the following form:

$$\gamma(\mathbf{n}) = \gamma_0\left\{1 - \sum_{i=1}^{M} \Delta\gamma_i \exp\left[-\frac{(l^2-l_i^2)^2 + (m^2-m_i^2)^2 + (n^2-n_i^2)^2}{p_i^4}\right]\right\}, \tag{4}$$

where γ_0 is the maximum value of the surface energy, the surface unit normal direction $\mathbf{n}=\{l,m,n\}$, and $\Delta\gamma_i$ and p_i are parameters which can be adjusted to create minima on the surface energy at surface normal directions $\{l_i,m_i,n_i\}$ for $i \in (1,M)$, where M is the number of directions with minimum surface energy. For the $Ge_xSi_{1-x}/Si(001)$ system model, the following faceted surfaces are used[5]: {100} and {501}.

The initial flat substrate surface is divided into a squared array. Within each of the squares, a hump adopting a cosine shape with a radius of r_0 and a height of H_0 is pre-patterned. Assume that (x_0,y_0) is the center of one of the squares and (x,y) is an arbitrary point within the square, then the hump shape is defined as

$$H(x,y) = \begin{cases} H_0 \cos[\pi\sqrt{(x-x_0)^2+(y-y_0)^2}/2r_0] & \text{if } \sqrt{(x-x_0)^2+(y-y_0)^2} \le r_0 \\ 0 & \text{if } \sqrt{(x-x_0)^2+(y-y_0)^2} > r_0. \end{cases} \tag{5}$$

The parametric studies here show that if r_0 is too large compared with λ_{cr}, the critical wavelength for surface roughness,[26,27] multiple dots may appear on the hump surface. However, if r_0 is too small compared with λ_{cr}, the dots sitting on the prepatterned humps may be unstable to a small perturbation in growth. Hence, focus is directed on the range in which r_0 is comparable to λ_{cr}.

Since GeSi/Si systems follow the Stranski-Krastanov growth mode, it is energetically unfavorable for the substrate to become exposed, that is, the film tends to wet the substrate surface. To model the wetting effect, a thin transition layer with a varying mismatch strain between the substrate and the fully strained film is introduced here.[37,42] It is assumed that the strain varies linearly, from the interface between the substrate and the transition layer, to the interface between the transitional layer and the fully strained film. Physically, the transition region can be thought of as a mixed phase of the thin film and substrate, giving rise to the variation of the mismatch strain.[37]

RESULTS AND DISCUSSIONS

Parametrical studies have been conducted by varying the system parameters. In the present simulations, the elastic modulus E, Poisson's ratio ν, and the elastic anisotropy strength assume the same values as silicon: that is, $E=47$ GPa, $\nu=0.218$ and $A=1.6$. It is found that SiGe surface {015} faceting can be modeled reasonably well if $\Delta\gamma_i=0.0012$ and $p_i=0.14$ for the minimum surface energy.

All numerical results will be presented in a dimensionless form. Lengths are normalized as $L_*=L/L_0$, where, $L_0=\gamma_0/\omega_0$, and ω_0 is the strain energy density on the initially flat (001) surface. The time scale is normalized by $t_*=t/t_0$, where $t_0=\gamma_0^3/(\Omega\omega_0^4D)$. In the present simulations, the dimensionless length and width of the simulation cells are both 40. The dimensionless substrate thickness is 16. The dimensionless transitional layer thickness is 0.1. The dimensionless parameters for the surface growth rate are chosen as $g_*=0.002$ and $\chi_v{}^*=5$. The normalized pitch distance P_* is the normalized lattice spacing for a prepatterned hump squared

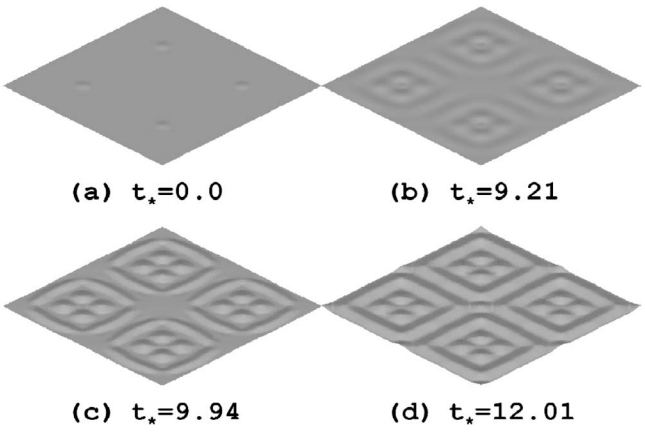

FIG. 1. Formation of island cluster surrounded by a fortress. $r_{0*}=2.0$, $H_{0*}=0.1$, $g_*=0.002$, $\chi_{v*}=5.0$, $P_*=20.0$, $\Delta\gamma_i=0.0012$, $p_i=0.14$, and $A=1.6$. The dimensionless simulation size is 40×40. (a) The initial prepatterned substrate surface, $t_*=0.0$; (b) the formation of double-ring structures, $t_*=9.21$; (c) the breakup of the inner ring into a cluster of islands, $t_*=9.94$; and (d) the formation of island cluster surrounded by a fortress, $t_*=12.01$.

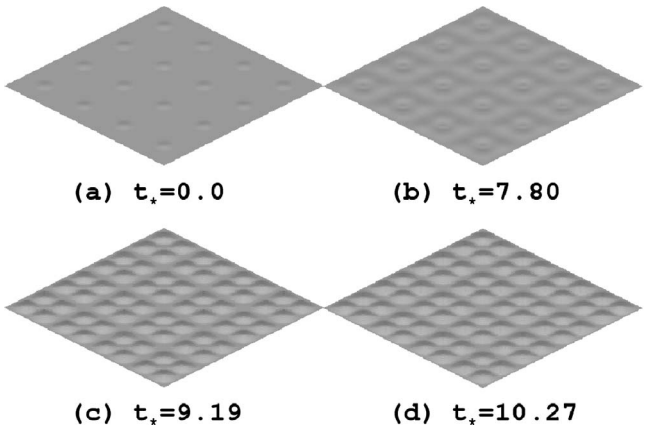

FIG. 2. Formation of island cluster. $P_*=10.0$ and all other parameters remain the same as in Fig. 1: (a) The initial prepatterned substrate surface, $t_*=0.0$; (b) the formation of single-ring structures, $t_*=7.80$; (c) the breakup of the ring into an island cluster, $t_*=9.19$; and (d) the formation of island clusters, $t_*=10.27$.

array. It should be noted that $\lambda_{cr^*}=\pi/(1+\nu)$, ν is the Poisson's ratio.

Figure 1 shows snapshots of the formation of surface structures grown on a prepatterned substrate surface. In the simulation, $r_{0^*}=2.0$, $H_{0^*}=0.1$, $g_*=0.002$, $\chi_{v^*}=5.0$, and $P_*=20.0$. Figure 1(a) shows the initial prepatterned substrate surface. At the early growth stage of growth, it is seen that each prepatterned hump is surrounded by a "fortress," which in turn is surrounded by another fortress [Fig. 1(b)]. The formation of the "double-fortress" structure is due to surface prepatterning which changes the surface chemical potential distribution. Our calculation shows that before deposition, the chemical potential is the highest at the top of the prepatterned humps, and is the lowest at the rim of the humps. The lowest chemical potential at these rims serves as an attractor for mass diffusion. Consequently, islands are formed around the humps rather than on the top of the humps. Thus it is the chemical potential distribution that drives the surface mass diffusion, leading to the formation of the double-fortress structures. The inner fortress breaks up into four {510} hut islands with further growth, but are still surrounded by the outer fortress. The four islands within the fortress are equal in size and aligned along the ⟨100⟩ directions [Fig. 1(c)]. This configuration is maintained as shown in Fig. 1(d) until the dimensionless growth time $t_*=12.5$. Afterwards, the four islands start to impinge with further growth and mergence occurs. This arrangement of these islands forms a basic cell of the quantum dot cellular automata, which demonstrates a nonlinear and bistable response and thus can be used for a transistorless approach to computation.[43,44]

The formation of the surface structures is strongly dependent on the pitch distance between the prepatterned humps. If the pitch distance is further increased, the four-island clusters surrounded by a fortress are still formed. However, additional islands are also formed in between the fortresses (not shown). The formation of the additional islands in between the fortresses can be explained by the fact that the distance between the fortresses is larger than the critical wavelength for surface roughness, and the mass deposited in between the fortress is able to accumulate and form those additional islands. If the pitch distance between the prepatterned humps is decreased by half, that is, $P_*=10.0$, as shown in Fig. 2(a), it is seen that each prepatterned hump is only surrounded by a single fortress, as shown in Fig. 2(b). Thus, there is no formation of the outer fortresses. The single fortress again breaks up into a cluster of four islands, resembling the quantum dot cellular automata. However, since there is no fortress surrounding the island cluster in this case, the packing density of the island clusters increased significantly. The formation of the island clusters without the surrounding fortress can be explained by the short distance between the prepatterned humps: the distance between the formed fortresses surrounding the humps is shorter than the critical wavelength for surface roughness, and the mass deposited in between is simply absorbed by the nearby fortresses. If the pitch distance is decreased further to $P_*=5.0$, a uniform and regular island array is formed, as shown in Fig. 3. These islands also adopt {510} faceted surfaces, as shown in Fig. 3(b). However, these islands prefer to locate at the positions right in between the prepatterned humps. Hence, the island density is the same as the prepatterned humps, but the island positions shift to the locations in between the humps.

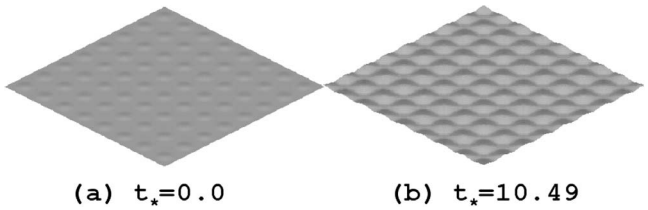

FIG. 3. Formation of a uniform and regular island array. $P_*=5.0$ and all other parameters remain the same as in Fig. 1: (a) The initial prepatterned substrate surface, $t_*=0.0$; (b) the formation of a uniform and regular island array with the same density as the prepatterned humps but at mismatch positions, $t_*=10.49$.

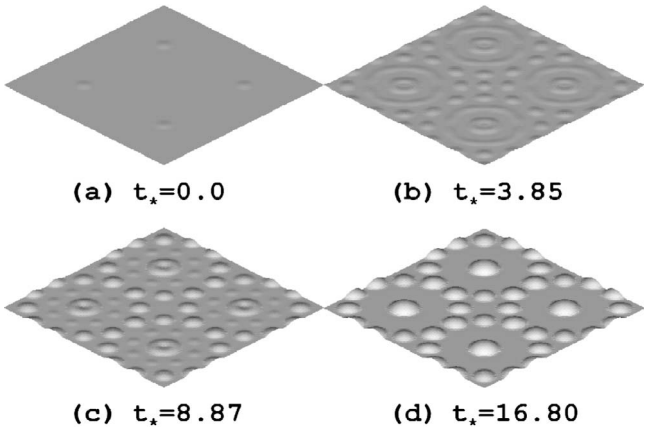

FIG. 4. Formation of surface structures. $P_*=20.0$ and the surface energy and elasticity are assumed to be isotropic. All other parameters remain the same as in Fig. 1: (a) The initial prepatterned substrate surface, $t_*=0.0$; (b) the formation of double-ring structures and islands in between the outer rings, $t_*=3.85$; (c) the breakup of the outer ring into islands, $t_*=8.87$; and (d) transformation of the inner ring into an island surrounded by islands lying in a circle, $t_*=16.8$.

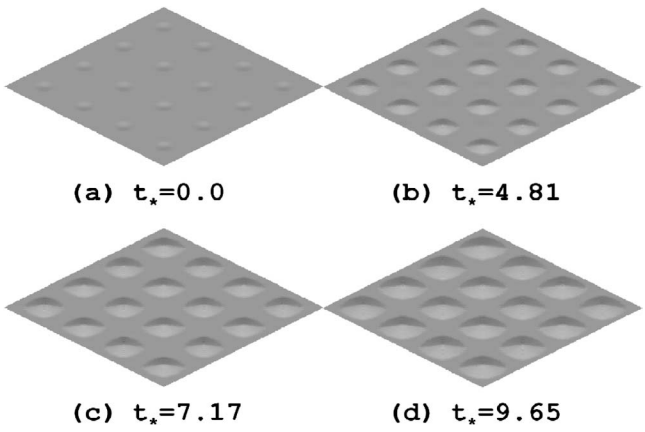

FIG. 5. Formation of an ordered island array. $H_{0^*}=-0.1$ and all other parameters remain the same as in Fig. 2: (a) The initial prepatterned substrate surface, $t_*=0.0$; (b) the formation of small hut islands with one-to-one relation, $t_*=4.81$; (c) the growth of hut islands, $t_*=7.17$; and (d) the growth of hut islands, $t_*=9.65$.

It is found that surface energy anisotropy and elastic anisotropy are important for creating surface structures. For Si, the elasticity anisotropy favors diffusion along ⟨100⟩ directions since the diffusion wavelength is the shortest along these directions.[9,40] Hence the fortresses are prone to aligning along the ⟨100⟩ directions under the influence of elastic anisotropy of Si. Surface energy anisotropy also changes the critical wavelength for surface roughness.[45] The introduction of the {510} faceted surfaces also favors surface alignment along the ⟨100⟩ direction and the formation of the {510} hut islands. If both surface energy and elasticity are assumed to be isotropic, and all other parameters remain to be the same, the formed surface structures are quite distinctive from those including both anisotropies. For example, the simulation result for $P_*=20.0$ without the two anisotropies is shown in Fig. 4. At an early stage of growth, a double-circular ring surface structure is observed for each prepatterned hump, as shown in Fig. 4(b). In addition, islands are also formed in between the circular rings. With further growth, the outer ring breaks up into islands, which subsequently shrink in size and disappear gradually, as shown in Figs. 4(c) and 4(d). The inner ring initially grows in size as shown in Fig. 4(c) and then transforms into an island as shown in Fig. 4(d). The islands initially formed in between the outer rings grow in size. The final pattern is that each prepatterned hump forms an island, which is surrounded by other islands lying in a circle as shown in Fig. 4(d). In this case, these islands adopt a spherical capped shape.

The parametric studies here show that the size and aspect ratio of the prepatterned humps are important factors in controlling surface patterns. If the lateral size of the humps is too large, multiple islands may develop on top of the hump surface. This type of island formation was both observed experimentally[33] and studied analytically.[35] To avoid multiple island formation on a prepatterned hump, r_{0^*} should not be too large compared with the critical wavelength for surface roughness ($\lambda_{cr^*}\approx 2.56$ for Si). Parametric studies show that the qualitative features of the formation of these surface structures are maintained if $1.0\leqslant r_{0^*}\leqslant 4.0$ and $0.015<H_{0^*}/r_{0^*}<0.125$. This growth window allows us to adjust the density of these surface features. It should be mentioned that the island (or the island cluster) density shown here is significantly higher than the currently experimentally achieved island densities. For example, for the Ge/Si system, if the mismatch strain is assumed to be 4%, Young's modulus 80 GPa, Poisson's ratio 0.28, and the surface energy 1.0 J/m^2, then the island density can be as high as 400 dots/μm^2. The currently experimentally achieved island density is only roughly 20 dots/μm^2 by Chen *et al.*[32] and 4 dots/μm^2 by Zhong *et al.*[33] Hence, there is still a large potential to increase the island (or the island cluster) density.

It should be mentioned that the growth pattern via pit prepatterning is distinctive from that via the hump prepatterning. Our preliminary study shows that if the sign of H_0 is negative (that is, pit prepatterning), and all other parameters remain unchanged, a one-to-one ordered island array may be easier to achieve. A typical example is shown in Fig. 5, in which $r_{0^*}=2.0$, $H_{0^*}=-0.1$, $g_*=0.002$, $\chi_{v^*}=5.0$, and $P_*=10.0$. Clearly a single island forms at each pit, forming a one pit–one dot relation. The formed surface pattern can be attributable to the chemical potential change during deposition: The lowest chemical potential on the prepatterned surface is located at the bottom of the pits, while the maximum chemical potential is at the rim of the pits. Interestingly, with further deposition, the chemical potential barrier at the pit rims gradually disappears, thus the deposited material can diffuse towards the pit centers (or dot tops at a later stage) without any diffusion barrier. With further growth, the chemical potential profile remains qualitatively the same. Hence at this stage, the dot tops serve as attractors for deposited mass due to the lack of diffusion barrier, ensuring the one-to-one relation.

SUMMARY

Surface prepatterning together with the surface energy anisotropy and elastic anisotropy strongly influences the formation of surface patterns during heteroepitaxial growth. Surface structures, such as quantum dot automata arrays, fortress-enclosed quantum dot automata arrays, and ordered quantum dot arrays, can be obtained by changing the pitch distance. The present work potentially provides a guideline for controlling the formation and self-assembly of surface structures.

*Author to whom correspondence should be addressed. FAX: 65-67763604. msezyw@nus.edu.sg

[1] J. A. Floro, G. A. Lucadamo, E. Chason, L. B. Freund, M. Sinclair, R. D. Twesten, and R. Q. Hwang, Phys. Rev. Lett. **80**, 4717 (1998).
[2] S. A. Chaparro, Y. Zhang, J. Drucker, D. Chandrasekhar, and D. J. Smith, J. Appl. Phys. **87**, 2245 (2000).
[3] A. Vailionis, B. Cho, G. Glass, P. Desjardins, D. G. Cahill, and J. E. Greene, Phys. Rev. Lett. **85**, 3672 (2000).
[4] D. E. Jesson, K. M. Chen, S. J. Pennycook, T. Thundat, and R. J. Warmack, Phys. Rev. Lett. **77**, 1330 (1996).
[5] F. M. Ross, R. M. Tromp, and M. C. Reuter, Science **286**, 1931 (1999).
[6] G. Medeiros-Ribeiro, A. M. Bratkovski, T. I. Kamins, D. A. A. Ohlberg, and R. S. Williams, Science **279**, 353 (1998).
[7] C. S. Ozkan, W. D. Nix, and H. J. Gao, Appl. Phys. Lett. **70**, 2247 (1997).
[8] H. Lee, J. A. Johnson, J. S. Speck, and P. M. Petroff, J. Vac. Sci. Technol. B **18**, 2193 (2000).
[9] Y. Obayashi and K. Shintani, J. Appl. Phys. **84**, 3141 (1998).
[10] Y. W. Zhang and A. F. Bower, Appl. Phys. Lett. **78**, 2706 (2001).
[11] J. Tersoff, B. J. Spencer, A. Rastelli, and H. von Kanel, Phys. Rev. Lett. **89**, 196104 (2002).
[12] H. R. Eisenberg and D. Kandel, Phys. Rev. B **71**, 115423 (2005).
[13] A. A. Golovin, M. S. Levine, T. V. Savina, and S. H. Davis, Phys. Rev. B **70**, 235342 (2004).
[14] A. A. Golovin, S. H. Davis, and P. W. Voorhees, Phys. Rev. E **68**, 056203 (2003).
[15] V. A. Shchukin, N. N. Ledentsov, P. S. Kop'ev, and D. Bimberg, Phys. Rev. Lett. **75**, 2968 (1995).
[16] J. E. Guyer and P. W. Voorhees, Phys. Rev. Lett. **74**, 4031 (1995).
[17] B. J. Spencer and J. Tersoff, Phys. Rev. Lett. **79**, 4858 (1997).
[18] H. T. Johnson and L. B. Freund, J. Appl. Phys. **81**, 6081 (1997).
[19] J. M. Baribeau, X. Wu, N. L. Rowell, and D. J. Lockwood, J. Phys.: Condens. Matter **18**, R139 (2006).
[20] Y. Y. Pang and R. Huang, Phys. Rev. B **74**, 075413 (2006).
[21] J. Drucker, IEEE J. Quantum Electron. **38**, 975 (2002).
[22] J. M. Baribeau, N. L. Rowell, and D. J. Lockwood, J. Mater. Res. **20**, 3278 (2005).
[23] L. H. Nguyen, T. K. Nguyen-Duc, V. Le Thanh, F. A. d'Avitaya and J. Derrien, Physica E (Amsterdam) **23**, 471 (2004).
[24] J. Martin-Sanchez, Y. Gonzalez, L. Gonzalez, M. Tello, R. Garcia, D. Granados, J. M. Garcia, and F. Briones, J. Cryst. Growth **284**, 313 (2005).
[25] T. S. Yoon, Z. M. Zhao, W. Feng, B. Y. Li, J. Liu, Y. H. Xie, D. Y. Ryu, T. P. Russell, H. M. Kim, and K. B. Kim, J. Cryst. Growth **290**, 369 (2006).
[26] S. C. Lee, A. Stintz, and S. R. J. Brueck, J. Appl. Phys. **91**, 3282 (2002).
[27] M. Borgstrom, V. Zela, and W. Seifert, Nanotechnology **14**, 264 (2003).
[28] S. Kiravittaya, H. Heidemeyer, and O. G. Schmidt, Physica E (Amsterdam) **23**, 253 (2004).
[29] R. Hull, J. L. Gray, M. Kammler, T. Vandervelde, T. Kobayashi, P. Kumar, T. Pernell, J. C. Bean, J. A. Floro, and F. M. Ross, Mater. Sci. Eng., B **101**, 1 (2003).
[30] A. Karmous, A. Cuenat, A. Ronda, I. Berbezier, S. Atha, and R. Hull, Appl. Phys. Lett. **85**, 6401 (2004).
[31] T. E. Vandervelde, P. Kumar, T. Kobayashi, J. L. Gray, T. Pernell, J. A. Floro, R. Hull, and J. C. Bean, Appl. Phys. Lett. **83**, 5205 (2003).
[32] G. Chen, H. Lichtenberger, F. Schaffler, G. Bauer, and W. Jantsch, Mater. Sci. Eng., C **26**, 795 (2006).
[33] Z. Y. Zhong, A. Halilovic, T. Fromherz, F. Schaffler, and G. Bauer, Appl. Phys. Lett. **82**, 4779 (2003).
[34] O. G. Schmidt, S. Kiravittaya, Y. Nakamura, H. Heidemeyer, R. Songmuang, C. Muller, N. Y. Jin-Phillipp, K. Eberl, H. Wawra, S. Christiansen, H. Grabeldinger, and H. Schweizer, Surf. Sci. **514**, 10 (2002).
[35] R. V. Kukta and D. Kouris, J. Appl. Phys. **97**, 033527 (2005).
[36] D. J. Srolovitz, Acta Metall. **37**, 621 (1989).
[37] R. V. Kukta and L. B. Freund, J. Mech. Phys. Solids **45**, 1835 (1997).
[38] H. J. Gao, J. Mech. Phys. Solids **42**, 741 (1994).
[39] J. Tersoff and R. M. Tromp, Phys. Rev. Lett. **70**, 2782 (1993).
[40] H. Gao, in *Modern Theory of Anisotropic Elasticity and Applications*, edited by J. J. Wu, T. C. T. Ting, and D. M. Barnett (SIAM, Philadelphia, PA, 1991), p. 139.
[41] C. S. Ozkan, W. D. Nix, and H. J. Gao, J. Mater. Res. **14**, 3247 (1999).
[42] P. Liu, Y. W. Zhang, and C. Lu, Phys. Rev. B **68**, 035402 (2003).
[43] A. O. Orlov, I. Amlani, G. H. Bernsein, C. S. Lent, and G. L. Snider, Science **277**, 928 (1997).
[44] G. L. Snipder, A. O. Orlov, I. Amlani, X. Zuo, G. H. Bernsein, C. S. Lent, and J. L. Merz, J. Appl. Phys. **85**, 4283 (1999).
[45] Y. W. Zhang, Phys. Rev. B **60**, 13325 (1999).